The Electrochemical Society
Advancing solid state & electrochemical science & technology

A Metal-Oxide Contact to ε-Ga$_2$O$_3$ Epitaxial Films and Relevant Conduction Mechanism

PRIME
PACIFIC RIM MEETING
ON ELECTROCHEMICAL
AND SOLID STATE SCIENCE
2020

Abstract Submission
DEADLINE EXTENDED:
May 29, 2020

Honolulu, HI | October 4-9, 2020

ECS

A Metal-Oxide Contact to ε-Ga$_2$O$_3$ Epitaxial Films and Relevant Conduction Mechanism

Alessio Bosio,[z] Carmine Borelli, Antonella Parisini, Maura Pavesi, Salvatore Vantaggio, and Roberto Fornari

Department of Mathematical, Physical and Computer Sciences, University of Parma, 43124 Parma, Italy

In this work, the conduction mechanisms across novel contacts to epitaxial films of pure phase epsilon-Ga$_2$O$_3$ (ε-Ga$_2$O$_3$) were investigated. Different structures made by sputtered metal and oxide thin films were tested as electrical contacts. I-V characteristics show heterogeneous behaviors, revealing different conduction mechanisms according to the applied bias. The results are interesting as they offer a viable method to obtain ohmic contacts on ε-Ga$_2$O$_3$, which is less studied than other gallium oxide polymorphs but may find application in new electronic and optoelectronic devices. The newly developed ohmic contacts allow to fabricate simple test devices and assess the potential of this material.

Wide-bandgap semiconductors, such as silicon carbide (SiC), gallium nitride (GaN) and gallium oxide (Ga$_2$O$_3$) have recently raised great interest thanks to their extraordinary physical properties.[1] A large energy bandgap, a high critical electric field and a small intrinsic carrier concentration make these materials suitable for the realization of electronic devices, which operate at temperature, voltage and frequency significantly higher than those based on silicon. Among these semiconductors, Ga$_2$O$_3$ is considered very attractive for the realization of power electronics,[2–6] short wavelength photonics,[7–9] gas sensors[10,11] and spintronics devices.[12]

Metal/semiconductor junction is the fundamental part of any electronic device, and its physical properties have a strong impact on the overall electrical performance. Consequently, a fundamental understanding of how contacts work is one of the main steps to achieve a successful device.

The carrier transport mechanism across the junction makes metal contacts either rectifying (Schottky) or nonrectifying (Ohmic). Ohmic contacts have linear and symmetric current-voltage (I-V) characteristic, while in a Schottky contact a potential barrier, inducing an asymmetric I-V profile, occurs.

Essentially, ohmic contacts with low contact resistance are required to reduce the on-resistance (R$_{on}$) in electronic power devices.[13,14] However, the realization of ohmic contacts on wide-bandgap semiconductors represents a real challenge.

Following the Schottky-Mott theory, a good ohmic contact with a *n*-type doped semiconductor is obtained only if the work function (Φ_m) of the metal, used as electrode, matches the electron affinity of the semiconductor (χ_s). If this condition is not satisfied, charge carriers have to overcome the (qΦ_m – χ_s) barrier height to be able to travel from semiconductor to metal. In order to avoid this situation, metals with low work function are commonly used.[1,15–17]

The preparation of ohmic contacts on β-Ga$_2$O$_3$ is well established and different structures, involving metals or oxide-based semiconductors, were proposed. Many studies have been already and some of these[18–22] have shown that for the realization of ohmic contacts the intermixing layer formed between the metal and β-Ga$_2$O$_3$ is crucial, rather the barrier height. For this reason, the formation of an intermediate semiconductor layer is stimulated by pre-treatments of the β-Ga$_2$O$_3$ film surface with plasma exposure,[6] reactive ion etching[5] and/or by post-contact deposition thermal annealing.[3,8,23] As an alternative to the formation of a thin small-gap semiconductor layer between the contact and the β-Ga$_2$O$_3$ layer, a heavily surface

doping via ion implantation of β-Ga$_2$O$_3$ was attempted.[6,24] When an elemental metal is used, an ohmic contact is normally obtained only when a post-deposition heat treatment at high temperature (800 °C–1000 °C) is made. This greatly restricts the choice of possible metals, because some of them react at high temperature with the Ga$_2$O$_3$ surface. Metal atoms can diffuse into Ga$_2$O$_3$, steal oxygen and form a thin insulating oxide layer. This process at the same time makes available free Ga atoms at the metal-Ga$_2$O$_3$ interface. As a consequence, a low melting point intermetallic layer is formed, which compromises the contact adhesion to Ga$_2$O$_3$ surface[18] and impedes the obtainment of a good contact.

In the case of orthorhombic ε-Ga$_2$O$_3$ polymorph, the use of high annealing temperature is not allowed, since the ε-phase is thermodynamically metastable. In fact, ε-Ga$_2$O$_3$ initiates a phase transformation at temperatures higher than 700 °C.[25]

On the other hand, ε-Ga$_2$O$_3$ is an interesting material with possible application in electronic and optoelectronic devices (i.e. solar-blind detectors), for this reason it is important to develop low-temperature processes for efficient electrical contacts on the ε-phase.

In this paper we present, for the first time, new results on the fabrication of ohmic contacts on nominally undoped ε-Ga$_2$O$_3$ grown by Metal Organic Chemical Vapour Deposition (MOCVD). Different stacked layers composed of metals and oxides were tested to achieve optimal metal-semiconductor-metal (MSM) devices adequate for UV-C detection. In particular, we explored the possibility to realize reliable contacts on resistive devices for UVC detector applications. For this purpose, it is mandatory to know if the contacts behave ohmic, independently from their mutual distance.

Experimental

The nominally undoped ε-Ga$_2$O$_3$ thin films utilized in this work were epitaxially grown by MOCVD on 2-inch c-oriented sapphire substrates. Room temperature (RT) resistivity of the samples was in the range ($10^6 \div 10^8$) Ω·cm (Table I). In order to prevent any surface effects, ε-Ga$_2$O$_3$ films were first etched in a solution of hydrofluoric and nitric acid (HF 50% + HNO$_3$ 50%) for 1 min and then sequentially rinsed in acetone, isopropanol, deionized water and finally dried in dry nitrogen.

The one-face planar geometry, used for the fabrication of the electrical contacts, is showed in Fig. 1. Contacts, with an area of (0.4 × 0.04) cm^2 spaced with nominal increasing distances of L$_1$ = 0.02 cm, L$_2$ = 0.04 cm, L$_3$ = 0.08 cm and L$_4$ = 0.16 cm between the contact strips, are realized by means of a stencil metallic mask.

[z]E-mail: alessio.bosio@unipr.it

Table I. Information related to investigated samples. Resistance is extrapolated from the slope of the I-V characteristics carried out on 4–5 pair, where the contribution of the material (ε-Ga$_2$O$_3$ film) between contacts dominates. Resistivity is estimated from resistance values by considering the geometrical dimensions; note that for 4–5 pair Rs $\gg$ R$_{C4}$ and R$_{C5}$. (S-B = Schottky-Barrier, P-F = Pool-Frenkel, TF-SCLC = Trap Free Space Charge Limited Current).

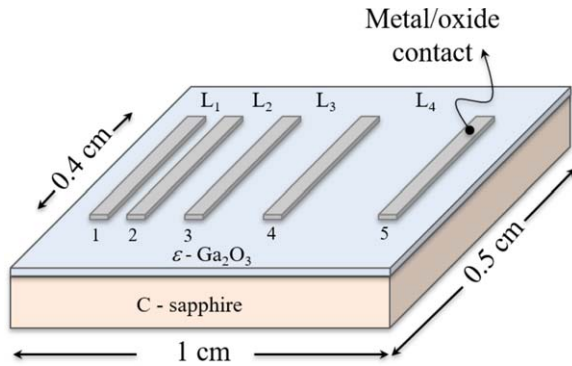| Sample	Thickness (nm)	Contact layers	RT Ga$_2$O$_3$ Resistance (4–5 pair) (Ω)	RT Ga$_2$O$_3$ Resistivity ($\Omega\cdot$cm)	Conduction model (1–2 pair)
#422 Ud1	290	SnO$_x$ + ITO	4×10^{10}	10^7	S-B
#475 Ud1	670	SnO$_x$ + ITO	5×10^9	10^6	P-F
#483 Ud1	930	SnO$_x$ + ITO	4×10^{11}	10^8	TF-SCLC

Figure 1. Contact configuration used for I-V measurements. L$_1$ = 0.02 cm, L$_2$ = 0.04 cm, L$_3$ = 0.08 cm and L$_4$ = 0.16 cm are the nominal distances between the contact strips.

In particular, metal films were deposited by direct current (d.c.) pulsed magnetron sputtering starting with 3-inch metal target. Ar ions were produced by applying a d.c. power density of 1.8 W cm^{-2} with a superimposed pulsed frequency of 100 kHz under an Ar pressure of 0.7 Pa. The resulted deposition rate was in the range of $(0.3 \div 0.5)$ nm s^{-1}.

Oxide films were deposited by a 13.56 MHz radio-frequency (r. f.) magnetron sputtering applying a r.f. power density of 0,7 W cm^{-2} over a 3-inch ceramic target under an Ar pressure of 0.3 Pa.

This sputtering system is equipped with a special tool for avoiding, as much as possible, the electron bombardment of the growing film. The ε-Ga$_2$O$_3$ film is covered by the incoming Sn and O atoms, which kinetic energy is carefully controlled by using low voltage drop (180 V) to keep the glow discharge on, corresponding to a very low deposition rate. The small energy provided by these atoms is just enough for increasing the surface temperature, allowing

the diffusion of Sn atoms into the very first superficial layer of the Ga$_2$O$_3$ film, but it is not sufficient to cause lattice damage.

Different metallization schemes, such as Ti/Au, ZnO/Ti/Au, ITO/Pt, realized on nominally undoped ε-Ga$_2$O$_3$ films, did not exhibit linear I-V characteristics at any temperature.

In both Ti/Au and ZnO/Ti/Au structures, the formation of a very resistive thin layer of titanium oxide TiO$_2$ at the interface between Ga$_2$O$_3$ and the contact layer occurs, already during the sputtering deposition. Although Ti forms an ohmic contact with β-Ga$_2$O$_3$, it is not thermodynamically stable with ε-Ga$_2$O$_3$. In fact, the free energy of formation of TiO$_2$ is more negative than that of ε-Ga$_2$O$_3$ resulting in the formation of an insulating oxide layer at the ε-Ga$_2$O$_3$/Ti interface. Even if the deposition is carried out at substrate temperatures as low as 80 °C, the energy of the sputtered Ti atoms impinging the surface of the Ga$_2$O$_3$ film may be higher than 10 eV. The surface thermalization of these atoms locally increases the temperature, leading to the formation of TiO$_2$.

Considering the ITO/Pt system, it is known that Pt could form PtO$_x$ inside the ITO matrix resulting effective in increasing the surface work function of the ITO film. In this condition the band alignment of Pt-doped ITO with ε-Ga$_2$O$_3$ rises the contact barrier causing a higher system resistance. Moreover, due to a weak sticking with the ε-Ga$_2$O$_3$ surface, the sputtered ITO film shows some cracks, which makes the procedure irreproducible and not usable. In order to avoid this problem, a sticking layer, consisting of a 100 nm thick SnO$_x$ film, is deposited by reactive sputtering on top of the ε-Ga$_2$O$_3$ layer prior to deposition of the ITO film.

Results and Discussion

In view of the considerations made in the Experimental section, the following discussion will be focused on the system SnO$_x$-ITO. The two layers, with a thickness of 100 nm and 1000 nm respectively, were sequentially deposited by sputtering on top of ε-Ga$_2$O$_3$ thin films.
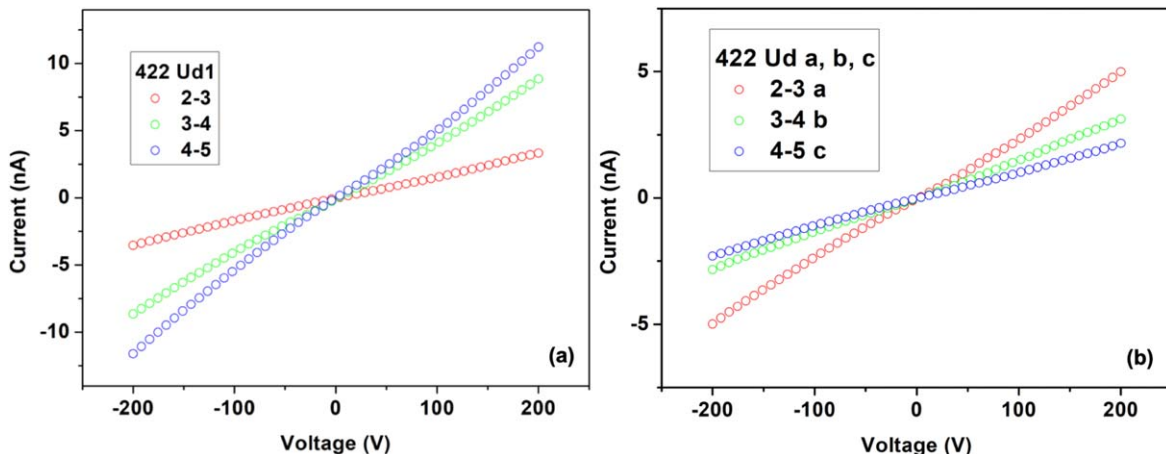

Figure 2. (a) Sample #422 Ud1, RT I-V characteristics measured on the 2–3, 3–4 and 4–5 pairs in non-stationary conditions; the slopes of the straight lines do not correspond to distances between the contact pads. (b) RT I-V characteristics of three different pieces (a)–(c) of the same layer (#422 Ud). In "a" only the 2–3 pair is contacted, while in "b" e "c" are contacted only the 3–4 and 4–5 pairs respectively; here the slopes of the straight lines do scale with the distances between the contact pads.
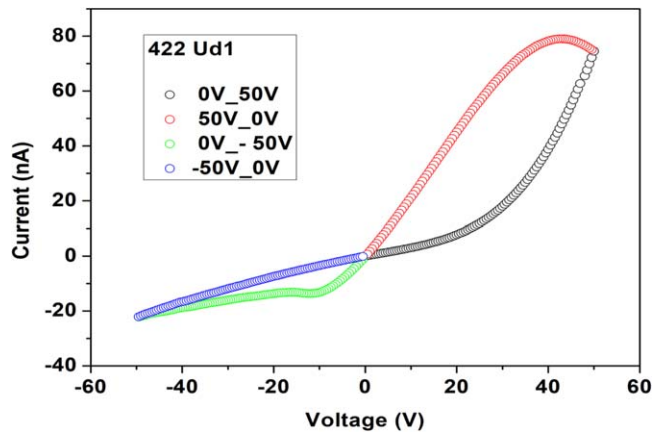
Figure 3. sample #422 Ud1, RT I-V characteristic measured on 1–2 contact pair in non-stationary conditions.

Voltage-sweep cycles (±50 V) and (±200 V) were applied to pairs of adjacent contacts and I-V characteristics were recorded at RT.

The first analysis, concerning 2–3, 3–4 and 4–5 pairs, exhibits a good ohmic behavior as it is shown in Fig. 2a. Nevertheless, the slopes of the curves, which give the conductance among the contacts under investigation, do not reflect the geometric distance between adjacent contacts.

If the measurement is performed in sequence, starting from 1–2 and then moving to 2–3, 3–4 and 4–5 pairs, space charge phenomena are observed. For example, the spatial charge effect on contact 2, triggered by the measurement on contact 1–2, also affects the 2–3 measurement, since contact 2 is common to both tests. This unwanted effect has been avoided by contacting three different specimens of the same ε-Ga$_2$O$_3$ layer (#422 Ud a,b,c) and then carrying out individual I-V measurement on just a pair for each specimen. The results are shown in Fig. 2b.

This spatial charge effect is more evident when the I-V characteristics are measured for the first time on as-grown samples. Actually, when the I-V measurement starts, the space charge builds up progressively, and the stationary condition is reached only after a certain time. This is well evidenced by the hysteresis of the I-V characteristics under positive bias sweep (from 0 V to 50 V and from 50 V to 0 V), Fig. 3 (black and red circles). Reversing the contact polarity, another trend is obtained (blue and green circles of Fig. 3), not symmetric with respect to the first cycle. In these conditions, the I-V characteristic changes continuously with time, making the study of the contact behavior very difficult.

Let us consider only the black circles of the I-V characteristic in Fig. 3, which correspond to the very first measurement performed on the 1–2 pair: two different trends are clearly visible: the first at low voltage, from 0 V to 20 V shows a linear behavior, while the second from 20 V to 200 V is compatible with a Schottky barrier- like behavior.

The linear part of the I-V characteristic, blown-up in Fig. 4a, is confirmed by a slope of 1.09 of the I-V plot in a Log-Log scale. This behavior may be explained by some mechanisms occurring at the interface between contact bi-layer and gallium oxide film: the SnO$_x$ contact releases some Sn atoms that diffuse into the Ga$_2$O$_3$ to provide *n*-type doping.[26] Tof-SIMS and RBS investigations (not reported here) show that sputtering deposition could promote the formation of a very thin intermixing layer, due to the interaction between Sn atoms and the surface of the Ga$_2$O$_3$ film.

As a consequence, a very thin barrier could form at the SnO$_x$/Ga$_2$O$_3$ interface due to the high concentration of donor atoms. In this situation, electrons, coming from SnO$_x$, may pass through the barrier thanks to a Fowler-Nordheim Tunneling or a Direct Tunneling mechanism. This hypothesis could explain the linear behavior of the first part of the I-V characteristic of the 1–2 pair. The

second part of the I-V characteristic, reported as Log I vs V$^{1/2}$ in Fig. 4b, shows the linear trend typical of Schottky or thermionic emission, which means a conduction mechanism ruled by:

$$I \propto T^2 \cdot \exp\left(a\, \frac{\sqrt{V}}{k_B T} - q\frac{\Phi_B}{k_B T} \right) \qquad [1]$$

Where T = absolute temperature, V = applied voltage, Φ_B = barrier height, k_B = Boltzmann constant and a is a constant that is independent on V and T but depends on the dynamic permittivity of ε-Ga$_2$O$_3$ and on the thickness of the conduction layer.

Why does the conduction mechanism change from tunneling through to passing over the potential barrier?

The Sn-doped interface layer, interposed between SnO$_x$ and undoped Ga$_2$O$_3$, as shown in Fig. 5a, plays a fundamental role for understanding the transition from linear to exponential conduction regime. The electron current through Ga$_2$O$_3$ is limited by the high resistance of the material and at low bias, only the weak tunneling current may flow. Increasing the applied potential, the current cannot increase proportionally, since electrons, coming from the contact, tend to accumulate widening the barrier and preventing tunneling. In this condition, conduction occurs by overcoming the barrier, following a Schottky-thermionic emission.

Moreover, it was observed that the electron current between adjacent contacts reaches a stationary condition only few minutes after having applied a certain voltage. This depends on the transient time necessary for stabilizing the space charge at the contact region.

The stationary condition is indeed reached faster by initially biasing the contact pairs for 5 min with high voltage (contact curing). That is 200 V for 5 min prior to voltage sweeps in the range (0 V ± 200 V). Following this procedure, the I-V characteristic of the 1–2 pair shows the behavior shown in Fig. 6. In the inset, the linear plot is explained by a Schottky-thermionic emission (Log I as a function of V$^{1/2}$), without tunneling (linear trend) typical of the I-V characteristics taken before the contacts curing at high voltage. In other words, submitting contacts to high voltage for few minutes, the space charge accumulated at one of the Sn-doped Ga$_2$O$_3$/undoped Ga$_2$O$_3$ interfaces reaches a stationary condition and the predominant conduction mechanism is well-described by a Schottky-thermionic emission over the entire voltage range.

A second question arises: why does this conduction mechanism take place just for the 1–2 pair, while the other contact couples exhibit a linear behavior independently from time and bias? Geometric distance between strips distinguishes different contact pair. As it is clearly seen in Fig. 1, this distance doubles passing from a contact couple to the adjacent one, starting from 0.02 cm for the 1–2 pair, arriving up to 0.16 cm for the 4–5 pair. The greater the distance the more Ga$_2$O$_3$ material contributes to the resistance between contacts. This consideration suggests a physical model on the distribution of the voltage drop (see Fig. 5b), which considers the resistances included between the contacts strips.[27,28]

When a voltage drop V is applied to a contact pair, we distinguish three main contributions. Denoting the voltage drop on the first contact (metal-semiconductor), on semiconductor, and on the second contact (semiconductor-metal) as V_{Ci}, V_s, V_{Cj}, respectively, the total voltage drop is: $V = V_{Ci} + V_S + V_{Cj}$, corresponding to a total resistance $R = R_{Ci} + R_S + R_{Cj}$.

In the case of 1–2 pair, the contact resistance R_{C1} and R_{C2} are greater than the material resistance R_S, accordingly, almost all the voltage falls on the contact barrier, symbolized by R_{C1} and R_{C2}. As a consequence, the contribution of the contacts is predominant. On the contrary, for other pairs the contribution of semiconductor resistance increases stepwise reaching soon the condition: $R_S \gg R_{C1}$ and R_{C2}. In this situation almost of the voltage drops on R_S and only a weak polarization falls on R_{C1} and R_{C2}. Low voltage means tunnelling through the contact barrier, corresponding to a linear behaviour in the I-V characteristic, and so is the contribution of R_S, purely ohmic.
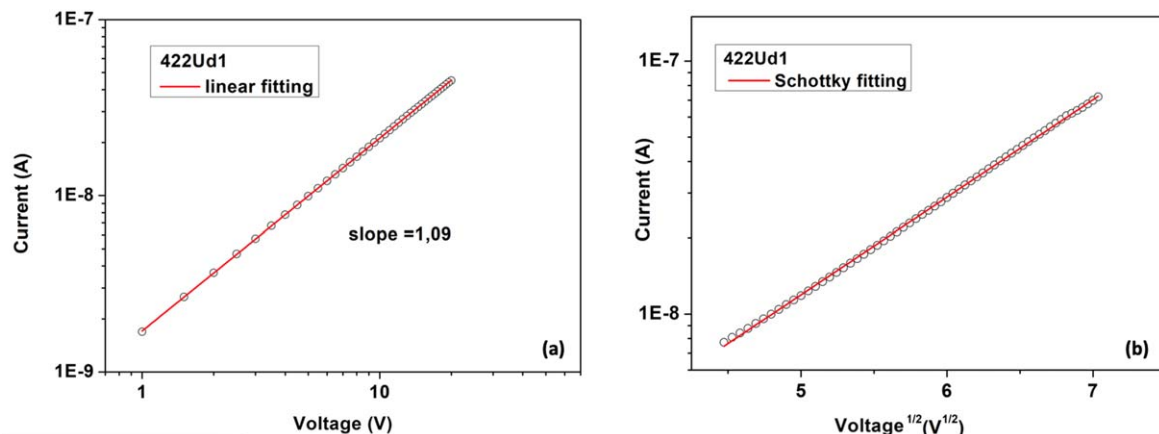
Figure 4. (a) RT I-V curve reported in Log-Log scale relative to Fig. 3 (black circles) for low-voltage sweeps from 0 V to 20 V, exhibiting a linear tunneling mechanism. (b) The second part of the same characteristic is reported in Log I vs $V^{1/2}$ scale for higher-voltage sweep (20 V to 50 V), showing a Schottky-like behavior.
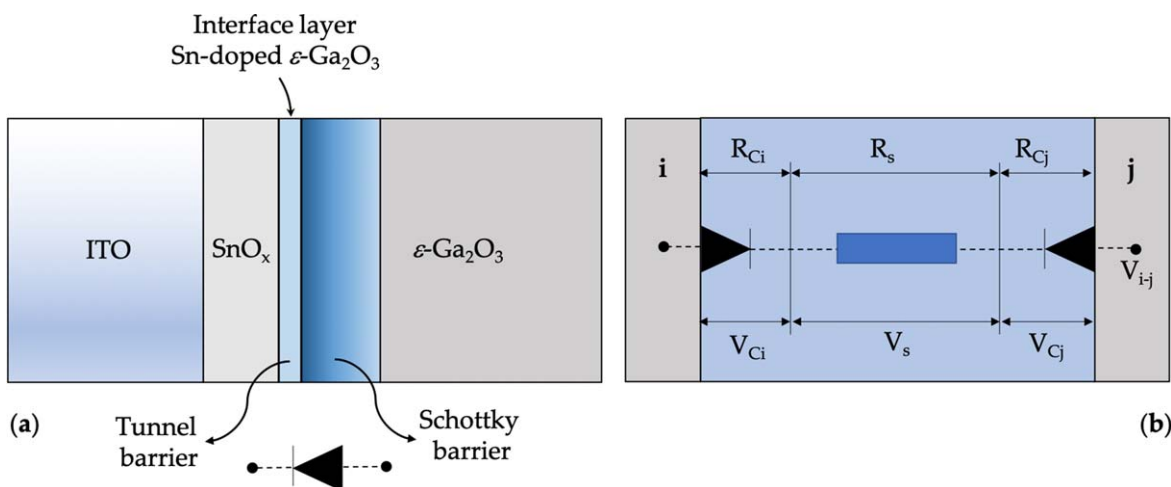

Figure 5. (a) Schematic of the ITO-SnOx contact to ε-Ga$_2$O$_3$ with the barrier formation at the interface layer. (b) schematic model for dual terminal ε-Ga$_2$O$_3$ system with highlighted the voltage drop distribution as a consequence of the resistive divider.
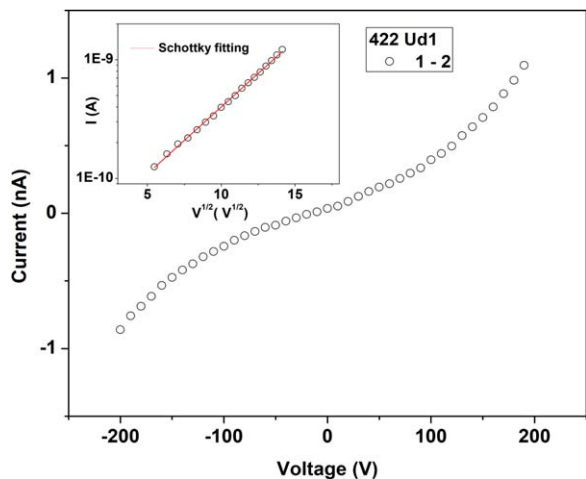

Figure 6. Sample #422 Ud1, RT I-V characteristic measured in stationary conditions, bias of 200 V for 5 min applied to the 1–2 pair. The inset shows Schottky conduction in the range 10 V–200 V. Current values under ±10 V bias are below the detectability treshold of the amperometer.

This explains the linearity of the I-V characteristics always observed for all contact pairs other than 1–2.

Several Ga$_2$O$_3$ samples were tested and different I-V characteristics were observed, which not always are well-fitted by Schottky barrier model. For all the samples, the I-V characteristics, related to the 1–2 pair, were performed in stationary conditions, i.e. after high potential had been applied for 5 min. As expected, the low-voltage linear behavior in experimental curves always disappeared, since the measurements were taken after high voltage curing. However, in some cases, the recorded I-V characteristic was consistent with space-charge limited current (SCLC) or Poole-Frenkel (P-F) emissions.[29,30]

SCLC mechanism is expected to occur in low mobility semiconductors, when injected charge density exceeds the intrinsic carrier density of the material. When the transport mechanism is described by the SCLC model, V and I are correlated by $I \propto V^m$ with $m \geqslant 2$. By plotting current and voltage values in Log-Log scale it is possible to determine the exponent m. For trap free (TF-SCLC) regime, $m = 2$ while for exponentially distributed trap (EDT-SCLC) regime $m > 2$.

For #483 Ud1 sample, experimental data (Fig. 7a) gave $m = 2, 04$ at RT, implying TF-SCLC regime.

P-F transport on the other hand is characterized by emission of trapped electrons into the conduction band, through thermal excitation enhanced by electric field. Conduction mechanism via the P-F model is described by:
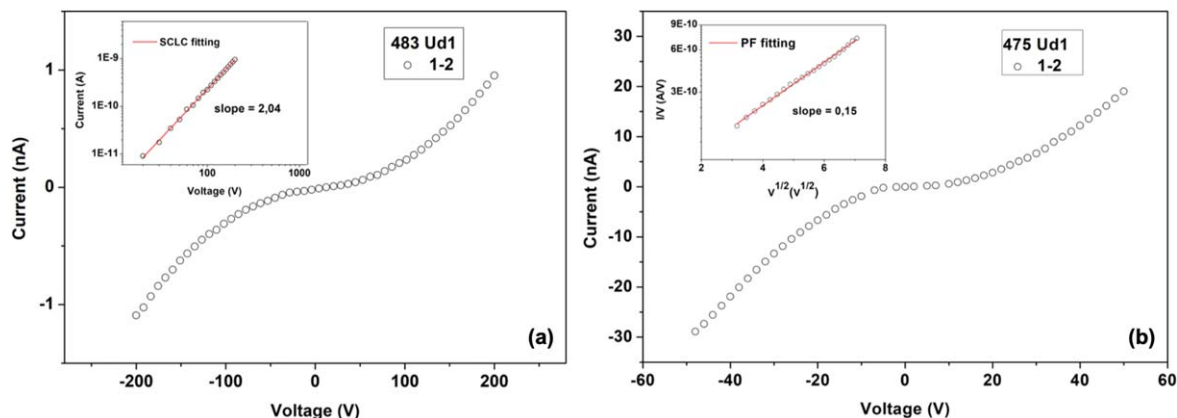
Figure 7. RT I-V characteristic measured between the 1–2 contacts, after preliminary curing at 200 V for 5 min (stationary condition) (a) sample #483 Ud 1, the inset is the fitting of the SCLC model in 10 V−200 V range. (b) sample #475 Ud 1. The inset represents the fitting of Pool-Frenkel model with positive applied bias; I-V characteristic is not completely symmetric with positive or negative bias since the contact pads are not identical.

$$I \propto V \cdot \exp\left(\frac{\beta\sqrt{V} - \phi}{K_B T}\right) \qquad [2]$$

where k_B and T have the usual meaning, ϕ is the barrier height of the trap and β is a coefficient related to the dielectric constant of the material ε_r by:

$$\beta = \sqrt{\frac{q^3}{d\pi\varepsilon_0\varepsilon_r}} \qquad [3]$$

where ε_0 is the vacuum permittivity and d is the width of the depletion region. For #475 Ud1 sample, the P-F model actually provides a good fit to the experimental data (Fig. 7b).

From Eq. 2 I-V curve should scale as Log (I/V) versus $V^{1/2}$. This plot yields a straight line with slope proportional to β. We can estimate the width of the depletion zone as $d \sim 40\,\mu$m, by considering $\varepsilon_r = 10$.

All the obtained results and the correlated conduction models are summarized in Table I.

It should be noted that, for all these electrical measurements no differences, attributable to conduction anisotropy were observed using contact patterns differently oriented on the surfaces of the Ga2O3 films. Anisotropy should not be expected anyway, as the epsilon structure, though orthorhombic at the microscopic scale, is indeed "hexagonal" at the scale typical of electronic transport.

Conclusion

Good ohmic contacts were achieved by deposition of SnO_x + ITO bilayers on undoped ε-Ga_2O_3 films grown by MOCVD on c-oriented sapphire. This is the first thorough investigation of this contact system applied to ε gallium oxide. Interestingly, the good ohmic behavior was obtained without making use of any high-temperature treatment, which is an indispensable requirement for fabrication of electronic devices based on the metastable ε-Ga_2O_3 polymorph. Experimental results show that the ohmic behavior is obtained when a low-voltage bias is applied. The ohmicity being attributed to tunneling through a very thin barrier at the interface between SnO_x and ε-Ga_2O_3 surface, formed in consequence of heavy Sn-diffusion from the deposited contact. At higher voltage bias a linear trend is achieved only if the two contacts are sufficiently distant, i.e. if the resistive contribution from Ga_2O_3 dominates over the contribution from contact strips.

If the interface barrier becomes too wide, the tunneling is not permitted and carriers overcoming the contact barrier provide the main contribution to the transport across the MSM structure. In this case three different models could explain the non-linearity trend of the I-V characteristics: two of these models are related to trap-free interface, i.e. the Schottky-thermionic and space charge limited current emissions; the third model bases on the Pool-Frenkel mechanism, that takes place when the depleted zone extends laterally over a larger part of the ε-Ga_2O_3 layer between the contacts.

ORCID

Alessio Bosio https://orcid.org/0000-0001-8572-454X

References

1. S. J. Pearton, J. Yang, P. H. Cary IV, F. Ren, J. Kim, M. J. Tadjer, and M. A. Mastro, *Appl. Phys. Rev.*, **5**, 1 (2018).
2. K. Irmscher, Z. Galazka, M. Pietsch, R. Uecker, and R. Fornari, *J. Appl. Phys.*, **110**, 063720 (2011).
3. K. Sasaki, A. Kuramata, T. Masui, E. G. Víllora, K. Shimamura, and S. Yamakoshi, *Appl. Phys. Express*, **5**, 5502 (2012).
4. S. Müller, H. von Wenckstern, F. Schmidt, D. Splith, F. L. Schein, H. Frenzel, and M. Grundmann, *Appl. Phys. Express*, **8** (2015).
5. M. Higashiwaki et al., *73rd Annual Device Research Conference (DRC)*, Piscataway, NJ(IEEE, Columbus, OH)**29** (2015).
6. M. H. Wong, K. Sasaki, A. Kuramata, S. Yamakoshi, and M. Higashiwaki, *IEEE Electr Device L*, **37**, 212 (2016).
7. T. Oshima, T. Okuno, N. Arai, N. Suzuki, S. Ohira, and S. Fujita, *Appl. Phys. Express*, **1**, 1202 (2008).
8. R. Suzuki, S. Nakagomi, Y. Kokubun, N. Arai, and S. Ohira, *Appl. Phys. Lett.*, **94**, 222102 (2009).
9. R. Suzuki, S. Nakagomi, and Y. Kokubun, *Appl. Phys. Lett.*, **98**, 131114 (2011).
10. M. Ogita, N. Saika, Y. Nakanishi, and Y. Hatanaka, *Appl. Surf. Sci.*, **142**, 188 (1999).
11. S. Nakagomi, T. Sai, and Y. Kokubun, *14th International Meeting on Chemical Sensors—IMCS 2012*, Nürnberg, DE, **750** (2012).
12. A. A. Dakhel and W. E. Alnaser, '*Microelectron Reliab*, **52**, 1050 (2012).
13. F. Roccaforte, F. La Via, and V. Raineri, *IJHSES*, **15**, 781 (2005).
14. B. J. Baliga, *Semicond. Sci. Technol.*, **28**, 074011 (2013).
15. J. S. Foresi and T. D. Moustakas, *Appl. Phys. Lett.*, **62**, 2859 (1993).
16. G. Greco, F. Iucolano, and F. Roccaforte, *App Surf Sci*, **383**, 324 (2016).
17. S. N. Mohammad, *J. Appl. Phys.*, **95**, 7940 (2004).
18. Y. Yao, R. F. Davis, and L. M. Porter, *J. Electron. Mater.*, **46**, 2053 (2017).
19. T. Oshima et al., *Jpn. J. Appl. Phys.*, **55**, 1 (2016).
20. S. Jang, S. Jung, K. Beers, J. Yang, F. Ren, A. Kuramata, S. J. Pearton, and K. H. Baik, *J Alloy Compd*, **731**, 118 (2018).
21. J. D. Guo, C. I. Lin, M. S. Feng, F. M. Pan, G. C. Chi, and C. T. Lee, *Appl. Phys. Lett.*, **68**, 235 (1996).
22. P. H. Carey, J. Yang, F. Ren, D. C. Hays, S. J. Pearton, S. Jang, A. Kuramata, and I. I. Kravchenko, *AIP Adv.*, **7**, 1 (2017).
23. T. Oshima, T. Okuno, N. Arai, N. Suzuki, H. Hino, and S. Fujita, *Jpn. J. Appl. Phys.*, **48**, 1605 (2009).
24. K. Sasaki, M. Higashiwaki, A. Kuramata, T. Masui, and S. Yamakoshi, *Appl. Phys. Express*, **6**, 6502 (2013).
25. R. Fornari et al., *Acta Mater.*, **140**, 411 (2017).

26. A. Parisini, A. Bosio, V. Montedoro, A. Gorreri, A. Lamperti, M. Bosi, G. Garulli, S. Vantaggio, and R. Fornari, *APL Mater*, **7**, 031114 (2019).
27. F. C. Chiu, *Adv. Mater. Sci. Eng.*, **1**, 2014 (2014).
28. Z. Zhang, K. Yao, Y. Liu, C. Jin, X. Liang, Q. Chen, and L. M. Peng, *Adv. Funct. Mater.*, **17**, 2478 (2007).
29. M. Choueib, A. Ayari, P. Vincent, S. Perisanu, and S. Purcell, *J. Appl. Phys.*, **109**, 073709 (2011).
30. D. Joung, A. Cunder, L. Zhai, and S. I. Khondaker, *Appl. Phys. Lett.*, **97**, 093105 (2010).